

ORIGINAL ARTICLE

# Reverse electrical remodeling following pressure unloading in a rat model of hypertension-induced left ventricular myocardial hypertrophy

Mihály Ruppert<sup>1,2</sup>, Sevil Korkmaz-Icöz<sup>1</sup>, Shiliang Li<sup>1</sup>, Béla Merkely<sup>2</sup>, Matthias Karck<sup>1</sup>, Tamás Radovits<sup>2,3</sup> and Gábor Szabó<sup>1,3</sup>

Pressure overload-induced left ventricular myocardial hypertrophy (LVH) is characterized by increased proarrhythmic vulnerability. In contrast, pressure unloading leads to reverse remodeling and decreases LVH-associated arrhythmogenicity. However, cellular changes that occur during reverse electrical remodeling have been studied less. Therefore, we aimed to provide an electrocardiographic characterization of a rat model of LVH that underwent pressure unloading and to simultaneously identify the underlying cellular and functional alterations. LVH was induced in rats by abdominal aortic banding for 6 or 12 weeks. Sham-operated animals served as controls. Pressure unloading was evoked by removing the aortic constriction after week 6 (debanded). Serial echocardiography and electrocardiography were performed to investigate the development and the regression of LVH. Protein expression levels were detected by western blot. Myocardial fibrosis was assessed by Picrosirius red staining. Pressure unloading resulted in the regression of LVH in correlation with the reversion of the prolonged corrected QT interval (cQT:  $68.7 \pm 1.6$  vs.  $91.0 \pm 1.9$  ms debanded week 12 vs. AB week 12,  $P < 0.05$ ). Furthermore, pressure unloading prevented the functional decompensation of LVH and simultaneously preserved adequate atrioventricular conduction (PQ:  $47.5 \pm 1.2$  vs.  $53.8 \pm 1.9$  ms debanded week 12 vs. AB week 12,  $P < 0.05$ ). Finally, pressure unloading effectively preceded the broadening of the QRS complex (QRS:  $21.8 \pm 0.5$  vs.  $24.9 \pm 0.7$  ms debanded week 12 vs. AB week 12,  $P < 0.05$ ) in parallel with the attenuation of interstitial collagen accumulation. The regression of LVH with maintained cardiac function and decreased myocardial fibrosis contributes to pressure unloading-induced reverse electrical remodeling.

*Hypertension Research* (2017) 40, 637–645; doi:10.1038/hr.2017.1; published online 26 January 2017

**Keywords:** left ventricular hypertrophy; pressure unloading; reverse electrical remodeling

## INTRODUCTION

Left ventricular (LV) myocardial hypertrophy (LVH) is the pathological response reaction of the heart to sustained pressure overload (hypertension and aortic stenosis) and it represents a major risk factor for the manifestation of ventricular tachyarrhythmias and sudden cardiac death.<sup>1</sup> As an explanation, the stimulus of chronic pressure overload not only induces increased expression of sarcomeric proteins with subsequent cardiomyocyte growth but also leads to distinct electrophysiological changes. These alterations are collectively termed electrical remodeling and involve altered expressions of  $\text{Ca}^{2+}$  handling proteins,<sup>2</sup> disrupted myocardial cell-to-cell coupling via decreased gap junction density<sup>3</sup> and enhanced interstitial fibrosis.<sup>4</sup> These adverse cellular changes occur at functionally different stages of LVH and provoke ventricular tachyarrhythmias by distinct pathomechanisms.

One of the most consistent electrophysiological findings in LVH is the prolongation of the action potential duration (APD)<sup>4</sup> that appears

on the ECG as a prolonged QT interval. In LVH, repolarization abnormalities that result from decreased trans-membrane outward potassium current<sup>5</sup> and increased inward  $\text{Ca}^{2+}$  current<sup>2</sup> were suggested as the cause for prolonged APD while creating the opportunity for early and late after depolarizations.<sup>6,7</sup> Indeed, it has been previously reported that triggered arrhythmias are the general pathomechanisms to induce sudden cardiac death in compensated LVH.<sup>4</sup>

Furthermore, functionally decompensated LVH and heart failure are commonly associated with a wide QRS complex,<sup>8</sup> which indicates a slowing of conduction. Among other things, the explanation for the disturbed conduction may originate from anatomical conduction blocks that are the result of increased myocardial fibrosis<sup>9</sup> and impaired cardiomyocyte-to-cardiomyocyte coupling as a function of adverse alterations of gap junctions.<sup>3</sup> In addition to the slowed conduction and delayed recovery from excitability, LVH is also characterized by dispersed refractoriness,<sup>10</sup> which collectively

<sup>1</sup>Department of Cardiac Surgery, University of Heidelberg, Heidelberg, Germany and <sup>2</sup>Experimental Research Laboratory, Heart and Vascular Center, Semmelweis University, Budapest, Hungary

<sup>3</sup>These authors contributed equally to this work.

Correspondence: Dr M Ruppert, Experimental Research Laboratory, Heart and Vascular Center, Semmelweis University, Városmajor u. 68., Budapest 1122, Hungary.

E-mail: ruppertmis@gmail.com

Received 10 September 2016; revised 18 November 2016; accepted 30 November 2016; published online 26 January 2017

predisposes the patient to re-entrant mechanisms of ventricular tachyarrhythmias.

In addition, the electrophysiological abnormalities in LVH and heart failure are not restricted to the ventricles. Prolongation of the PR interval was recently reported in a rabbit model of congestive heart failure, which showed an anatomical enlargement of the atrioventricular junction and specific changes in ion-channel expressions.<sup>11</sup>

On the other hand, termination of the pathological stimulus of sustained hemodynamic overload at an early stage can lead to reverse myocardial remodeling,<sup>12,13</sup> which may include beneficial electrophysiological consequences as well. Indeed, clear evidence of reverse electrical remodeling has been provided by Rials *et al.*,<sup>14</sup> who found that the regression of LVH by pressure unloading was associated with a significantly lowered incidence of inducible polymorphic ventricular arrhythmia, a higher fibrillation threshold and normalized monophasic APD in an aortic-banded feline model. However, despite an extensive literature search, no existing data is currently available concerning the mechanisms of reverse electrical remodeling.

Therefore, the aims of this study were (1) to provide an electrocardiographic characterization of the development and the regression of LVH by pressure unloading in an aortic-banded rat model and (2) to identify the underlying cellular and functional alterations in reverse electrical remodeling.

## METHODS

### Animals

Male Sprague-Dawley rats ( $n=51$ ) (160–180 g; Charles River, Sulzfeld, Germany) were housed in a room with constant temperature of  $22 \pm 2^\circ\text{C}$  with 12-h light/dark cycles. During the 12-week-long observation period, the animals were allowed access to a standard laboratory rat diet and water ad libitum. All animals received humane care in compliance with the 'Principles of Laboratory Animal Care' formulated by the National Society for Medical Research and the 'Guide for the Care and Use of Laboratory Animals' prepared by the Institute of Laboratory Animal Resources and published by the National Institutes of Health (NIH Publication No. 86–23, revised 1996). This investigation was approved by the appropriate ethics review committee.

### Abdominal aortic banding and debanding procedures

Pressure overload was induced by abdominal aortic banding ( $n=33$ ), as previously described.<sup>15,16</sup> Briefly and under isoflurane anesthesia, a midline laparotomy was performed and the abdominal aorta was constricted to the external diameter of a 22-gauge needle at the suprarenal level by a 2-0 silk suture.<sup>17</sup> Following surgery, analgesia was provided by subcutaneously administered buprenorphine at a dose of  $0.05\text{ mg kg}^{-1}$ . Sham-operated animals ( $n=18$ ) were subjected to the same surgical procedure without the completion of the aortic constriction.

In the group of aortic-banded animals ( $n=11$ ), the narrowing suture was cut and removed from the abdominal aorta after experimental week 6. A prompt drop of blood pressure was confirmed by simultaneous invasive blood pressure measurement via the carotid artery during the debanding procedure as was also observed in previous pilot studies.

### Experimental groups and design

Six weeks after the aortic banding or sham operation, the animals were divided into five experimental groups:

- (1) Aortic-banded week 6 group ( $n=8$ ): after undergoing aortic banding, these animals received followed-up for a 6-week-long experimental period;
- (2) Sham-operated week 6 group ( $n=8$ ): after undergoing a sham operation, these animals received followed-up for a 6-week-long experimental period;
- (3) Aortic-banded week 12 group ( $n=14$ ): after undergoing aortic banding, these animals received followed-up for a 12-week-long experimental period;

- (4) Sham-operated week 12 group ( $n=10$ ): after undergoing a sham operation, these animals received followed-up for a 12-week-long experimental period;
- (5) Debanding week 12 group ( $n=11$ ): these animals underwent the aortic banding procedure, and after week 6, the banding suture was removed, and these animals were followed up until week 12.

To investigate the time course of the electrical, morphological and hemodynamic alterations of the hearts, serial electrocardiography and echocardiography were performed after weeks 3, 6, 9 and 12. At the end of the experimental period (week 6 or 12), invasive blood pressure measurement was conducted. Afterwards, the rats were killed, the hearts and the lungs were removed and the heart weights (HW) and lung weights (LW) were immediately measured and normalized to the tibial length (HW/TL, LW/TL).

### Echocardiography

Echocardiography was performed as previously described.<sup>18</sup> In brief, anesthesia was induced with 5% isoflurane in a chamber. Once sedated and while in a supine position, the animals were placed on an automatic heating pad to maintain their body temperatures at  $37^\circ\text{C}$  and were also connected to a funnel to maintain the inhalational anesthesia of 1.5–2% isoflurane gas in  $\text{O}_2$ . To gain an appropriate acoustic window, the thorax of the animals was shaved and a pre-warmed ultrasound gel was applied. Then, transthoracic echocardiography was performed by using an HDI 5000 CV echocardiography machine (ATL Ultrasound, Philips, Bothell, WA, USA) equipped with a 10 MHz linear probe. Two-dimensional parasternal long-axis and short-axis images as well as M-mode recordings at the mid-papillary muscle level were assessed. The study was completed by analyzing the digital images in a blinded fashion using image analyzing software (HDI Lab, Philips, Bothell, WA, USA).

From these images, the following parameters were measured: LV anterior wall thickness (AWT), LV posterior wall thickness (PWT) in diastole (index: d) and systole (index: s); LV end-diastolic (LVEDD) and end-systolic (LVESD) diameters. End-diastolic and end-systolic time points were defined, as were the largest and the smallest dimension of the LV. All values were calculated as the average of three consecutive cardiac cycles.

LV mass was calculated to estimate myocardial weight using the Devereux formula:  $\text{LV mass (g)} = \{[(\text{LVEDD} + \text{AWT}_d + \text{PWT}_d)^3 - \text{LVEDD}^3] \times 1.04\} \times 0.8 + 0.14$ .<sup>19</sup> In addition, LV volumes were estimated according to the prolate method:  $\text{LVEDV} = [(3.14/6) \times \text{LVEDD}^2] \times \text{L}$ .<sup>20</sup> Cardiac function was assessed using the following parameters: fractional shortening (FS) as  $[(\text{LVEDD} - \text{LVESD})/\text{LVEDD}] \times 100$  and ejection fraction (EF) as  $(\text{LVEDV} - \text{LVESV})/\text{LVEDV} \times 100$ .

### Electrocardiography

After echocardiography, standard 12-lead ECGs were recorded using needle electrodes placed subcutaneously.<sup>18</sup> All leads were connected to a standard direct-writing recorder (Mortara Instrument, Milwaukee, WI, USA). The paper speed was set at  $50\text{ mm s}^{-1}$ , and the sensitivity was set at  $10\text{ mm mV}^{-1}$ . The ECG analysis was evaluated in lead II, which included the following measurements: heart rates, PQ intervals and the duration of both the QRS complex and QT intervals. The QT interval was measured from the first deflection of the QRS complex to the end of the T wave and was corrected using the normalized Bazett's formula adjusted for rats to achieve the QTc ( $\text{nQTc} = \text{QT}/(\text{RR}/f)^{1/2}$ ).<sup>21</sup> An investigator blinded to the experimental groups analyzed the electrocardiography.

### Invasive hemodynamic measurement

After the experimental period (week 6 or 12), invasive hemodynamic measurement was performed.<sup>15</sup> The rats were anaesthetized with sodium pentobarbital ( $60\text{ mg kg}^{-1}$  i.p.), tracheotomized and intubated to facilitate breathing. The animals were then placed on an automatic heating pad in a supine position, and the body temperature was maintained (measured via a rectal probe) at  $37^\circ\text{C}$  during the entire procedure. A polyethylene catheter was inserted into the left external jugular vein for fluid administration. A 2F microtip pressure microcatheter (SPR-838, Millar Instruments, Houston, Tx, USA) was inserted into the right carotid artery and advanced into the ascending

aorta. After 5 min of stabilization, the systolic arterial blood pressure, diastolic arterial blood pressure and mean arterial pressure were recorded. Then, the catheter was advanced to the LV under pressure control. After another 5 min of stabilization, LV pressure–volume loops were recorded. From the generated pressure–volume data, LV end-systolic pressure and LV end-diastolic pressure were automatically calculated using Millar's PVAN software. After completion of the hemodynamic measurements, all animals were killed by exsanguination.

### Histology

After the hemodynamic measurements were completed, all rats were killed by exsanguination, and the hearts were explanted. Pieces of LV myocardial tissue were fixed in a buffered paraformaldehyde solution (4%) and embedded in paraffin. Transverse, transmural, 5 µm thick slices of the ventricles were sectioned and placed on adhesive slides. The sections were stained with hematoxylin and eosin to detect the diameter of the cardiomyocyte, which served as a marker for myocardial hypertrophy. In each sample, 100 longitudinally oriented cardiomyocytes from the LV were examined, and the diameters at the transnuclear position were defined. The mean value of 100 measurements represented one sample. An assessment of myocardial fibrosis was carried out by Picrosirius red staining. The collagen accumulation in the myocardium was determined by semi-quantitative morphometry scoring of the sections according to the following: 0: absent, 1: slight, 2: moderate and 3: intense. Twenty randomly selected visual fields of the LV were assessed, and the mean value is representative of one sample. An investigator blinded to the experimental design conducted the evaluations.

### Western blotting

Western blotting was performed as previously described.<sup>22</sup> Heart-tissue samples were lysed with a RIPA buffer (Melford, Ipswich, UK) to release the proteins of interest. Bradford measurements were used to determine the protein concentrations. In semi-dry conditions, a total of 20 µg/30 µl protein homogenates were denatured at 70 °C, separated on sodium dodecyl sulfate polyacrylamide electrophoresis gels and transferred to polyvinylidene fluoride membranes (Millipore, Darmstadt, Germany). After transfer, the membranes were washed and blocked for 1 h in a 5% solution of bovine serum albumin in Tris-buffered saline Tween 20 at room temperature to reduce the non-specific binding of the antibodies. The membranes were then incubated overnight at 4 °C with the following primary antibodies: anti-Connexin43 (Cx43) antibody (1:1000 dilution, Abcam, Cambridge, UK), anti-L-type Ca<sup>2+</sup> Channel Protein α1C (LTCC) antibody (1:500 dilution, Santa Cruz Biotechnology, Heidelberg, Germany) and an anti-sarcoplasmic/endoplasmic reticulum Ca<sup>2+</sup>-ATPase 2 (SERCA2) antibody (1:1000 dilution, Abcam). The blots were washed to remove excessive primary antibody binding and incubated with a horseradish peroxidase-conjugated secondary antibody (1:5000 dilution, Santa Cruz Biotechnology) for 1 h at room temperature. The glyceraldehyde-3-phosphate dehydrogenase housekeeping protein was used for loading control and protein normalization. The immunoreactive protein bands were developed using the Enhanced Chemiluminescence system (PerkinElmer, Rodgau-Juegesheim,

Germany). The intensity of the immunoblot bands was detected with the Chemi-smart™ 5100 system (Peqlab, Biotechnologie, GmbH, Erlangen, Germany).

### Statistics

All values are expressed as the mean ± s.e.m. The normal distribution of our data was tested using the Shapiro–Wilk test. In the case of normally distributed data sets, one-way analysis of variance (ANOVA) followed by Tukey's *post hoc* test was used for detecting differences among groups. Data sets that failed to show normal distribution were analyzed by the nonparametric Kruskal–Wallis test followed by Dunn's *post hoc* test. Repeated measures one-way ANOVAs followed by Tukey's *post hoc* tests were performed to compare data of the electrocardiographic and echocardiographic measurements at four time points within a group. Correlations between LV mass and cQT interval, CD and cQT interval, HW/TL ratio and cQT interval, fibrosis score and QRS complex duration, Cx43 expression level and QRS complex duration, EF and PQ interval, FS and PQ interval, and LW/TL ratio and PQ interval were detected using Spearman correlation tests. A *P*-value of <0.05 was used as the criterion for statistical significance.

## RESULTS

### Effect of banding and debanding of the aorta on arterial blood pressure

Banding of the abdominal aorta resulted in significantly increased systolic blood pressure, diastolic blood pressure and mean arterial pressure in weeks 6 and 12 aortic banding groups (Table 1). In contrast, removing the narrowing suture after week 6 in the week 12 debanded group significantly reduced these parameters (Table 1).

### Myocardial remodeling and pressure unloading-induced reverse remodeling

In the aortic-banded group, LVH had already developed after experimental week 3, as detected by significantly increased LV mass index values (Table 2). The cardiomyocyte growth showed further progression in week 6, which was confirmed by significantly increased LV mass, CD and HW/TL ratio (Table 1 and Figures 1a,b and 3b). The myocardial collagen content did not differ in the week 6 aortic-banded group when compared with the control as revealed by Picrosirius red staining (Figures 1a and c). The hypertrophied hearts after 6 weeks of pressure overload proved to be functionally compensated, as reflected by maintained EF and FS (Table 2 and Figure 3d).

The decompensation of cardiac function in the aortic-banded group started after week 9 and became even more pronounced at the end of the 12-week-long experimental period. Near the end of the experimental period, EF and FS were significantly reduced, whereas LVESV was significantly increased when compared with the week 6 state in the

**Table 1 Basic parameters**

	Sham 6th week	Sham 12th week	AB 6th week	AB 12th week	Debanded 12th week
Heart weight, g	1.25 ± 0.02	1.54 ± 0.05	2.08 ± 0.10*	2.49 ± 0.07**	1.70 ± 0.08#
HW/TL, g cm <sup>-1</sup>	0.31 ± 0.01	0.35 ± 0.01	0.50 ± 0.02*	0.57 ± 0.02**	0.38 ± 0.02#
Lung weight, g	1.49 ± 0.06	1.83 ± 0.03	1.82 ± 0.06	2.12 ± 0.19	1.90 ± 0.05
LW/TL, g cm <sup>-1</sup>	0.37 ± 0.02	0.41 ± 0.01	0.44 ± 0.01	0.48 ± 0.04	0.43 ± 0.01
SBP, mmHg	144 ± 3	143 ± 5	224 ± 8*	201 ± 9*	173 ± 5**
DBP, mmHg	117 ± 2	118 ± 3	158 ± 4*	153 ± 5*	135 ± 3**
MAP, mmHg	126 ± 2	126 ± 3	180 ± 4*	171 ± 6*	148 ± 3**
LVESP, mmHg	133.4 ± 5.9	121.0 ± 7.4	195.8 ± 8.5*	184.0 ± 7.7*	166.0 ± 3.8**
LVEDP, mmHg	4.5 ± 0.6	5.5 ± 0.6	5.8 ± 1.0	8.2 ± 1.4	5.6 ± 0.4

Abbreviations: AB, aortic banded; DBP, diastolic blood pressure; HW/TL, heart weight/tibial length; LVEDP, left ventricular (LV) end-diastolic pressure; LVESP, left ventricular (LV) end-systolic pressure; LW/TL, lung weight/tibial length; MAP, mean arterial pressure; SBP, systolic blood pressure.

All values are expressed as means ± s.e.m. \**P*<0.05 vs. age-matched sham, #*P*<0.05 vs. aortic-banded 6th week, \*\**P*<0.05 vs. aortic-banded 12th week.

**Table 2** Echocardiographic parameters during the development and the regression of LV hypertrophy

	Sham (n = 10)	Aortic banded (n = 14)	Debanded (n = 11)
<i>Third week</i>			
Body weight, g	370 ± 8	354 ± 5	350 ± 11
LV mass index, g kg <sup>-1</sup>	2.60 ± 0.08	4.52 ± 0.18*	4.85 ± 0.22*
LVEDV, µl	441.79 ± 19.75	412.24 ± 16.02	471.63 ± 20.89
LVESV, µl	133.32 ± 9.69	113.53 ± 7.26	138.09 ± 11.22
FS, %	39.40 ± 1.27	43.80 ± 1.28	42.14 ± 1.28
HR, beats min <sup>-1</sup>	341 ± 13	357 ± 7	358 ± 9
<i>Sixth week time of debanding</i>			
Body weight, g	467 ± 7 <sup>†</sup>	450 ± 11 <sup>†</sup>	471 ± 17 <sup>†</sup>
LV mass index, g kg <sup>-1</sup>	2.76 ± 0.07	4.70 ± 0.14*	4.35 ± 0.19*
LVEDV, µl	605.62 ± 24.45 <sup>†</sup>	628.45 ± 19.75 <sup>†</sup>	625.25 ± 28.38 <sup>†</sup>
LVESV, µl	198.60 ± 7.27 <sup>†</sup>	223.19 ± 21.50 <sup>†</sup>	201.25 ± 13.43 <sup>†</sup>
FS, %	38.66 ± 1.31	37.99 ± 1.77	39.76 ± 1.16
HR, beats min <sup>-1</sup>	337 ± 10	363 ± 12	355 ± 13
<i>Ninth week</i>			
Body weight, g	527 ± 9 <sup>†‡</sup>	518 ± 14 <sup>†‡</sup>	482 ± 14 <sup>†</sup>
LV mass index, g kg <sup>-1</sup>	2.52 ± 0.08 <sup>‡</sup>	4.59 ± 0.21*	3.33 ± 0.15 <sup>#†‡</sup>
LVEDV, µl	618.67 ± 14.59 <sup>†</sup>	708.34 ± 36.59 <sup>†‡</sup>	619.75 ± 29.54 <sup>†</sup>
LVESV, µl	197.82 ± 11.37 <sup>†</sup>	350.09 ± 34.13 <sup>*†‡</sup>	210.55 ± 14.14 <sup>#†</sup>
FS, %	40.34 ± 1.43	28.15 ± 1.56 <sup>*†‡</sup>	38.60 ± 1.06 <sup>#†</sup>
HR, beats min <sup>-1</sup>	339 ± 15	353 ± 8	331 ± 9
<i>Twelfth week</i>			
Body weight, g	569 ± 10 <sup>†‡§</sup>	556 ± 13 <sup>†‡§</sup>	542 ± 17 <sup>†‡§</sup>
LV mass index, g kg <sup>-1</sup>	2.47 ± 0.08	4.21 ± 0.20 <sup>*‡§</sup>	2.90 ± 0.12 <sup>#†‡§</sup>
LVEDV, µl	653.00 ± 18.09 <sup>†</sup>	759.58 ± 38.87 <sup>†‡</sup>	657.12 ± 26.14 <sup>†‡</sup>
LVESV, µl	207.96 ± 12.20 <sup>†</sup>	404.58 ± 40.24 <sup>*†‡</sup>	208.19 ± 16.11 <sup>#†</sup>
FS, %	39.62 ± 1.28	25.27 ± 1.72 <sup>*†‡</sup>	39.95 ± 1.33 <sup>#</sup>
HR, beats min <sup>-1</sup>	328 ± 14	366 ± 9	363 ± 11

Abbreviations: FS, fractional shortening; HR, heart rate; LVEDV, LV end-diastolic volume; LVESV, LV end-systolic volume; LV mass index, left ventricular mass index. All values are expressed as means ± s.e.m. \**P* < 0.05 vs. sham, #*P* < 0.05 vs. aortic-banded, <sup>†</sup>*P* < 0.05 vs. 3rd week, <sup>‡</sup>*P* < 0.05 vs. 6th week, <sup>§</sup>*P* < 0.05 vs. 9th week.

aortic-banded group (Table 2 and Figure 3d). In addition, LV mass, CD, HW/TL ratio, as well as myocardial fibrosis significantly increased in the week 12 aortic-banded group when compared with the control and to the week 6 aortic-banded group (Table 1 and Figures 1a–c and 3b). Furthermore, LV end-diastolic pressure and LW/TL ratio also increased with a strong tendency, however, testing of these variables did not reach the level of statistical significance (Table 1).

Pressure unloading resulted in significantly decreased LV mass, CD, HW/TL ratio (Table 1 and Figures 1a,b and 3b) and extracellular matrix collagen accumulation (Figures 1a and c) in the week 12 debanded group when compared with the week 12 aortic-banded group. Furthermore, pressure unloading protected the heart from functional deterioration as reflected by the maintained EF and FS (Table 2 and Figure 3b).

#### Electrocardiographic characterization of electrical remodeling and reverse remodeling

In the aortic-banded group, significant QT prolongation was already detectable after the third experimental week and showed further progression for weeks 6, 9 and 12 (Figures 2 and 3a). The QT prolongation showed a strong correlation with the incremental rise in LV mass (Figure 4a), CD (Spearman *r* = 0.6332, *P* < 0.0001) and HW/TL ratio (Spearman *r* = 0.8864, *P* < 0.0001).

Furthermore, a significantly elongated PQ interval was also observed in the aortic-banded group beginning in week 9 (Figures 2 and 3c). Significant correlations were detected between the PQ interval and EF (Figure 4b), FS (Spearman *r* = -0.2874, *P* = 0.0006), and LW/TL ratio (Spearman *r* = 0.2889, *P* = 0.0441).

In addition, the QRS complex was significantly widened at the weeks 6 and 12 time points in the aortic-banded group (Figures 2 and 3e). The width of the QRS complex proved to correlate with the fibrosis score as detected by Picrosirius red staining (Figure 4c), whereas no correlation could be observed between the QRS complex and Cx43 expression levels (Spearman *r* = -0.04027, *P* = 0.8327).

Pressure unloading provided substantial protection against all the electrical changes seen in the aortic-banded group, including the prolonged QT and PQ intervals and the widened QRS complex (Figures 2 and 3).

#### Electrical remodeling and reverse remodeling was associated with distinct protein expression profile

Western blot analysis revealed that the protein expression level of Cx43 decreased with a strong tendency, but statistical significance was neither achieved in the week 6 nor in the week 12 aortic-banded groups. In the debanded group, the tendency was restored to the level of the control (Figure 5a). The expression level of LTCC remained unchanged in all experimental groups (Figure 5b). In contrast, and

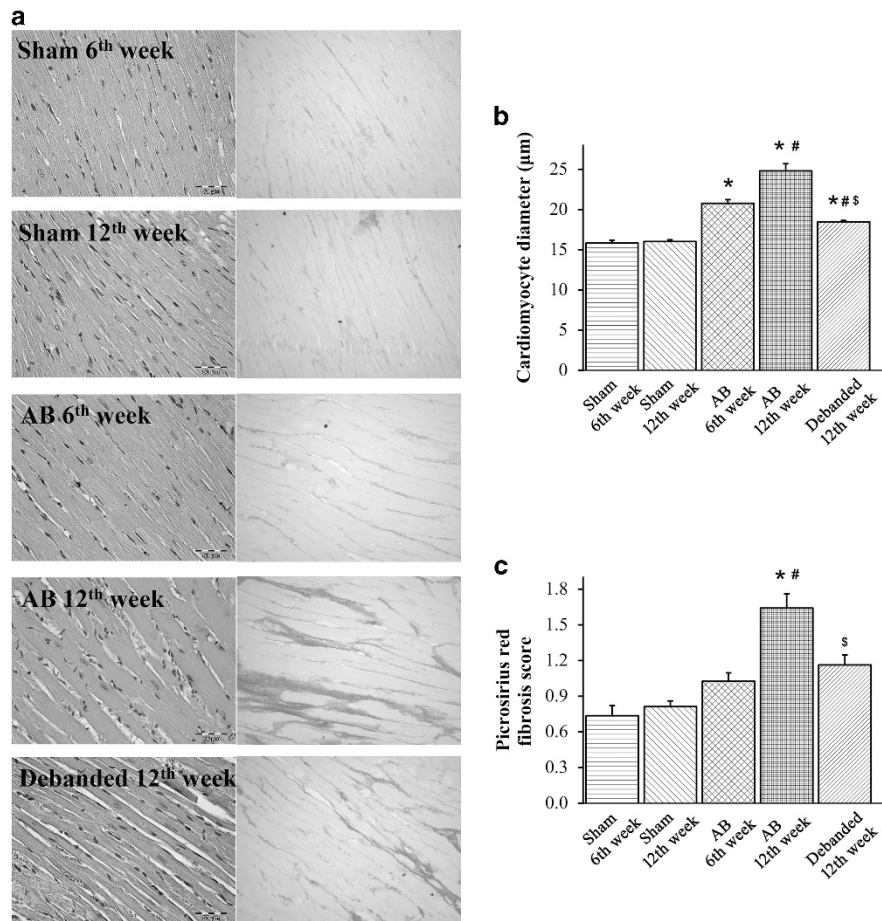


**Figure 1** Myocardial remodeling and pressure unloading-induced reverse remodeling. LVH was detected by significantly increased cardiomyocyte diameter (CD) in the weeks 6 and 12 aortic-banded groups (**a, b**). However, pressure unloading led to a significant reduction of increased CD, indicating regression of LVH (**a, b**). Furthermore, while myocardial fibrosis proved to be significantly increased in the aortic-banded week 12 group, pressure unloading effectively inhibited the collagen accumulation in the interstitium (**a, c**). The representative photomicrographs (**a**) were stained with hematoxylin and eosin and Picrosirius red, respectively. Magnification  $\times 20$ , scale bar,  $50\ \mu\text{m}$ . All values are expressed as the means  $\pm$  s.e.m. \* $P < 0.05$  vs. age-matched sham, # $P < 0.05$  vs. aortic-banded week 6, \$ $P < 0.05$  vs. aortic-banded week 12. A full color version of this figure is available at the *Hypertension Research* journal online.

due to the sustained pressure overload, the protein level of SERCA2 exhibited a strong decreasing tendency in the week 6 aortic-banded group, which became even more pronounced in the week 12 aortic-banded group. The tendency of SERCA2 expression in the week 12 debanded group was restored to the level of the control (Figure 5c).

## DISCUSSION

In this study, we aimed to provide an electrocardiographic characterization of a rat model of LVH that underwent pressure unloading therapy and to identify the underlying mechanisms during reverse electrical remodeling. To the best of our knowledge, this was the first study that demonstrated a relationship between the restoration of abnormal ECG findings and the cellular and functional alterations during the regression of LVH.

### Pressure unloading restored the prolonged QT interval in tandem with the regression of LVH

Prolongation of APD has been reported as one of the most common electrophysiological finding in LVH.<sup>4</sup> Elongated APD appears as a prolonged QT interval on the ECG, which manifests in tandem with the development of LVH, according to prior studies.<sup>23,24</sup> In our

experiment, LVH had already developed after week 3 of sustained pressure overload and it showed a strong correlation with the prolongation of the cQT interval (Figures 2,3 and 4a). Furthermore, the progression of LVH for experimental weeks 6, 9 and 12 was confirmed by significantly increased LV mass, HW/TL and CD (Table 1 and Figures 1a,b and 3b) that entailed further elongation of the QT interval in the week 12 aortic-banded group (Figures 2 and 3a).

Delayed repolarization due to decreased outward potassium current and increased inward calcium current has been identified as the underlying pathomechanism for the QT prolongation in LVH.<sup>2,5</sup> The pathophysiology describes the duration of action potential is mainly determined by the repolarization period, which is dependent on two antagonistic ion currents. On one hand, the activation of the outward potassium currents leads to prompt repolarization in the sarcolemma.<sup>25</sup> However, this is immediately counterbalanced by the influx of  $\text{Ca}^{2+}$  via voltage-gated ion channels.<sup>25</sup> Subsequently, the gradual intensification of activated potassium currents and the closure of  $\text{Ca}^{2+}$  channels tip the balance toward repolarization. Consequently, precise regulation of these two opposite ion currents is required to ensure a physiological QT interval.

In contrast, there is less consensus concerning the alterations of the Ca<sup>2+</sup> currents in LVH and heart failure with potassium channel remodeling. Depending on the severity of LVH, augmentation,<sup>26</sup> no change<sup>26</sup> or even reduction<sup>27</sup> was reported in the availability and in the expression level of LTCC. Furthermore, studies that utilized human heart failure samples concluded that despite the reduced myocardial LTCC expression, the Ca<sup>2+</sup> current appears to be maintained because of increased phosphorylation of the channel.<sup>27</sup> In rodents, alterations in Ca<sup>2+</sup> cycling proteins were identified as the main determinants for the increased inward calcium current in LVH. In a pressure overload-induced LVH guinea pig model, a reduction in SERCA2 expression was predicted to induce decreased sarcoplasmic reticulum (SR) Ca<sup>2+</sup> load and consequently diminished the SR Ca<sup>2+</sup>-induced Ca<sup>2+</sup> release to the cytoplasm. This led to reduced Ca<sup>2+</sup>-dependent inactivation of the LTCC.<sup>2</sup> In our study, the expression level of LTCC remained unchanged in the aortic-banded groups, despite the chronic pressure overload (Figure 5b). However, the protein level of SERCA2 showed a strong tendency toward reduced values in weeks 6 and 12 aortic-banded groups (Figure 5c). Therefore, the indirect enhancement of the LTCC current via decreased SERCA2 expression might have contributed to the prolongation of the QT interval in our model.

At the same time, pressure unloading resulted in a significant regression of LVH, as reflected by the reduced LV mass, HW/TL and CD (Table 1 and Figures 1a,b and 3b), and simultaneously led to the normalization of the prolonged QT interval (Figures 2 and 3a). As the underlying molecular alteration, a strong increasing tendency in the SERCA2 protein expression level, was identified in the week 12 debanding group (Figure 5c) compared with the week 12 aortic-banded group.

### Pressure unloading protected the heart from functional decompensation and inhibited PQ interval prolongation

Contrary to the QT interval and in our investigation, the prolongation of the PQ interval did not follow incremental changes in LV mass, but showed a correlation with the functional deterioration of LVH (Figure 4b). In concordance with our findings, a prolonged PR interval (from the first deflection of the P wave until the beginning of the R wave) in association with anatomical enlargement of the atrioventricular junction and expression alterations in distinct ion channels has been recently reported in a congestive heart failure rabbit model with poor cardiac function and pulmonary edema.<sup>11</sup>

In our investigation, the functional decompensation in the aortic-banded animals started after week 9 of sustained pressure overload and was characterized by significantly decreased EF and FS (Table 2 and Figure 3b). In addition, the strong and increased tendencies of LV end-diastolic pressure and the LW/TL ratios in the week 12 aortic-banded group provided evident signs of diastolic dysfunction and backward heart failure (Table 1) in our pressure-overloaded rat model, which is analogous to prior observations.<sup>28</sup> The impairment of cardiac function (decreased EF and FS, increased LW/TL ratio) showed a correlation with the prolongation of the PQ interval (Figure 4b), which also became significantly prolonged after week 9 in the aortic-banded animals (Figure 3c). Therefore, we hypothesize that the secondary increased pressure load on the atria due to decreased LV performance may have been responsible for the manifestation of the prolonged PQ interval.

On the other hand, pressure unloading effectively inhibited the functional deterioration of LVH and prevented the elongation of the PQ interval (Figures 3c and d and Table 2).

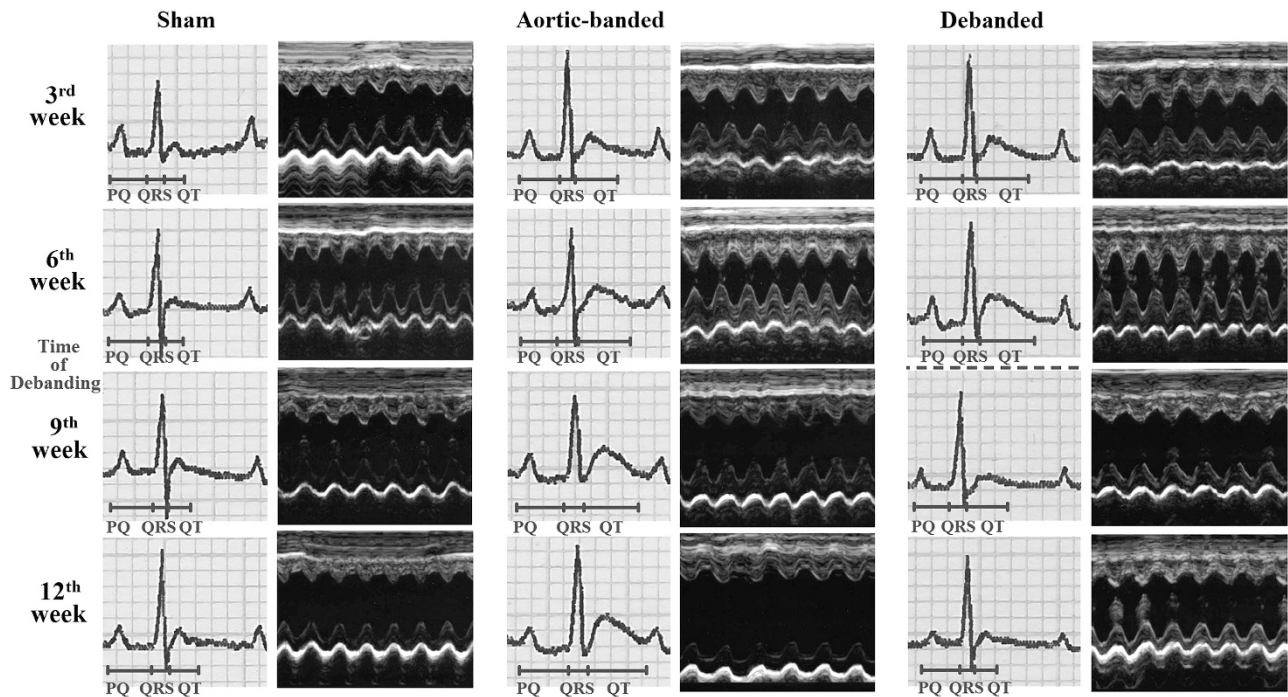


**Figure 2** Representative echocardiographic pictures and electrocardiographic recordings during the development and regression of LVH. Representative M-mode echocardiographic images at the mid-papillary muscle level and ECG recordings in lead II are shown, demonstrating the morphological/functional and electrical alterations during the temporal development of LVH and its regression by pressure unloading. A full color version of this figure is available at the *Hypertension Research* journal online.

**Pressure unloading prevented the widening of the QRS complex along with reduced myocardial fibrosis and restored Connexin43 expression**

Wide QRS complex is a frequently diagnosed ECG abnormality among patients with severe heart failure,<sup>8</sup> which also proved to be a predictor of mortality in this patient population.<sup>29</sup> The wide QRS complex on the ECG indicated a conduction slowdown in the ventricles. Under physiological conditions, the co-existence of two main factors ensures normal propagation of the electrical impulse among the cells.

First, the adequate density of the gap junctions within the intercalated disks, where the single cardiomyocytes are connected to each other by low-resistant pores represent one of the heart's intercellular channels whereby Cx43 is one of the most important components.<sup>30</sup> Therefore, the pathogenetic role of Cx43 in heart failure-associated arrhythmogenesis has been under intense investigation. Numerous studies reported a decreased expression of Cx43 in failing human heart samples of different etiologies.<sup>31,32</sup> However, the level of Cx43 in compensated LVH proved to be unchanged or even

increased.<sup>31</sup> In contrast, and in an aortic-banded rat model, LVH was associated with the re-localization of Cx43 from the intercalated disks to the entire cell surface.<sup>33</sup> The dispersion of Cx43 resulted in a relative deficit of Cx43 in the intercalated disks. In our model, Cx43 expression showed a decreasing tendency in the weeks 6 and 12 aortic-banding groups although it did not reach the level of statistical significance (Figure 5a).

Also required for the adequate connection among the cardiomyocytes is the second main factor, which is the low amount of interstitial fibrosis.<sup>4</sup> Although appropriate collagen architecture in the interstitium is necessary to build the scaffold of the heart, the exaggerated extracellular matrix accumulation can lead to a disruption of the cell-to-cell connections, which results in impaired conduction.<sup>9</sup> In our study, week 6 aortic-banded group was associated with a normal collagen content. However, significantly enhanced myocardial fibrosis was certified in the week 12 aortic-banded group (Figures 1a and c).

In our investigation, the widening of the QRS complex showed a significant correlation with the extent of myocardial fibrosis

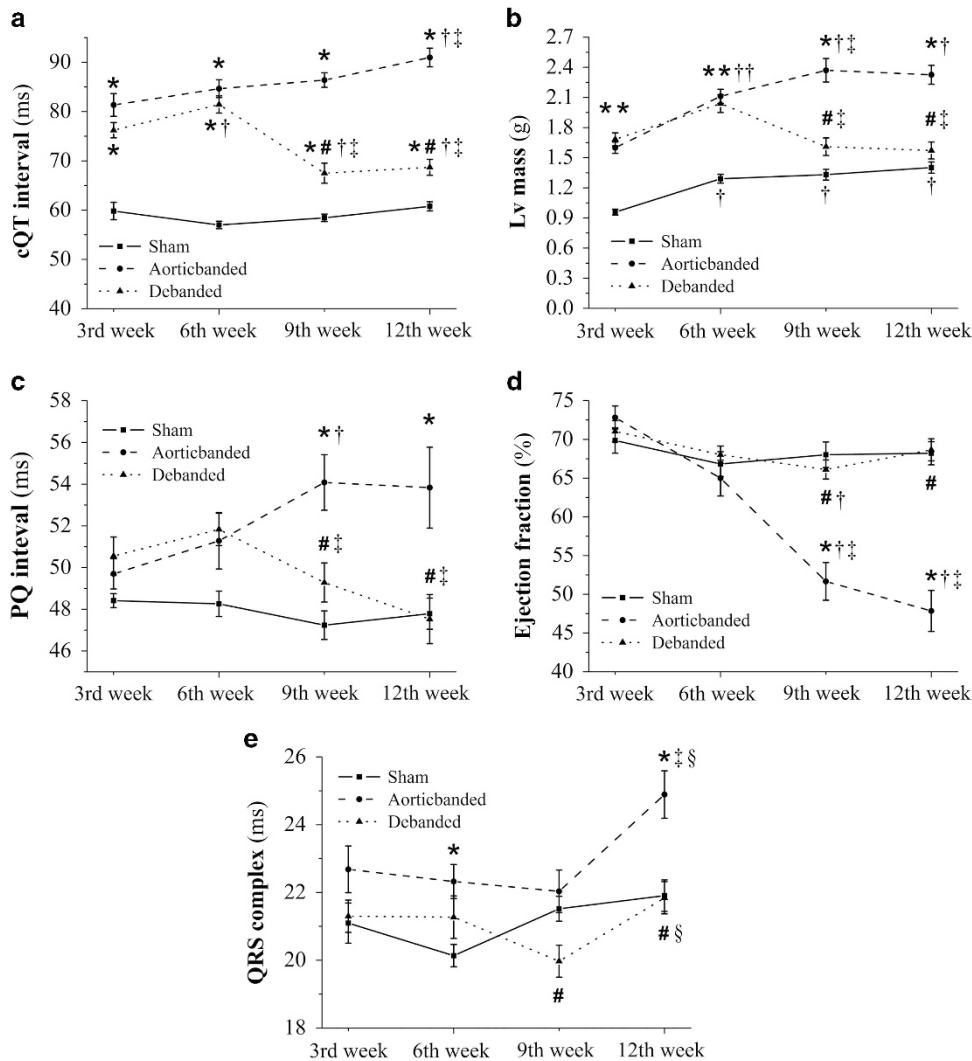


**Figure 3** Time course of the electrical, morphological and functional alterations during the development and regression of LVH. Because of the sustained pressure overload, the cQT interval and LV mass had already increased after week 3 and showed further progression for weeks 6, 9 and 12 (a, b). In contrast, the prolongation of the PQ interval, as well as the reduction of the EF, appeared after experimental week 9 (c, d). Finally, widening of the QRS complex became evident after week 6 of sustained pressure overload (e). LV mass indicates left ventricular (LV) mass. All values are expressed as the means  $\pm$  s.e.m. \* $P < 0.05$  vs. sham, # $P < 0.05$  vs. aortic-banded, † $P < 0.05$  vs. 3rd week, ‡ $P < 0.05$  vs. 6th week, § $P < 0.05$  vs. 9th week.

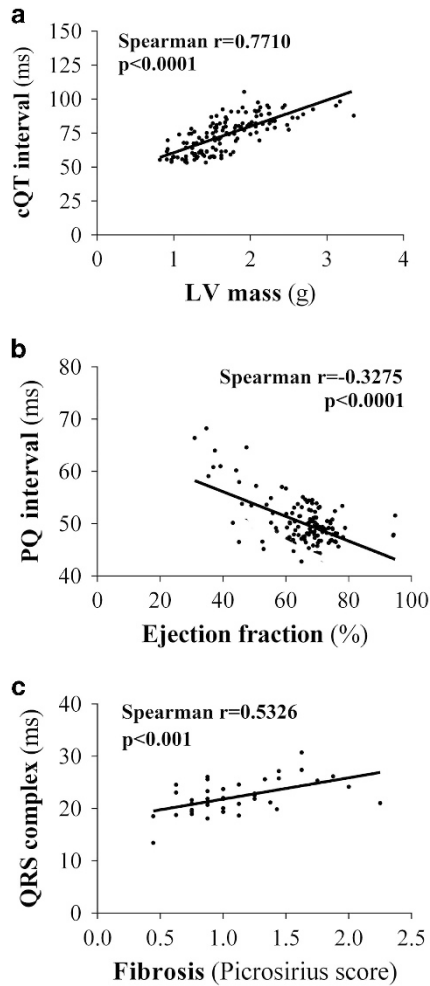


**Figure 4** Correlation between the ECG findings, and the morphological and functional alterations during the development and regression of LVH. The increment of LV mass showed a strong correlation with the prolongation of the cQT interval (a). In addition, an inverse correlation was detected between the EF and the PQ interval (b). Finally, the extent of myocardial fibrosis proved to be correlated with the QRS width (c). LV mass indicates left ventricular (LV) mass.

(Figure 4c). In contrast, the protein expression level of Cx43 failed to correlate with the duration of the QRS complex. Therefore, in our study, the enhanced collagen accumulation between cardiomyocytes might be the main contributor of slowed electrical impulse propagation.

On the other hand, pressure unloading prevented fibrotic alterations in the myocardium (Figures 1a and c) and restored the expression of Cx43 (Figure 5a), which ultimately provided protection against the manifestation of the broadened QRS complex while normal conduction was maintained.

### CONCLUSION

In our experiment, pressure overload-induced LVH was associated with prolonged QT and PQ intervals, and widened QRS complexes. The ECG abnormalities appeared at functionally different stages of LVH with diverse cellular and functional pathomechanisms. The prolongation of the QT interval correlated well with the development of LVH, and therefore, was already present in the compensated form of LVH. The decreased expression of SERCA2 was identified as the main molecular mechanism underlying the elongated QT interval. Furthermore, the prolongation of the PQ interval appeared to correspond with the functional decompensation of LVH. In addition, we found that increased myocardial fibrosis—rather than decreased expression of Cx43—was responsible for the impaired conduction propagation as reflected by the widened QRS complex.

Conversely, pressure unloading resulted in a significant regression of LVH, which was accompanied by the restoration of SERCA2 expression and the reduction of the prolonged QT interval. Moreover, pressure unloading maintained the functionality of the left ventricle and therefore preserved atrioventricular synchrony as reflected by the reduced PQ interval. Finally, by attenuating the myocardial collagen accumulation and by increasing the expression of Cx43, pressure unloading effectively preceded the broadening of the QRS complex.

### Study limitations

The interpretation of results from this study is limited to young male rats. The possible influence of gender, age or species should be assessed in future studies.

Although the electrophysiological principles in humans and rodents are identical, certain differences can be found in heart rate, APD and

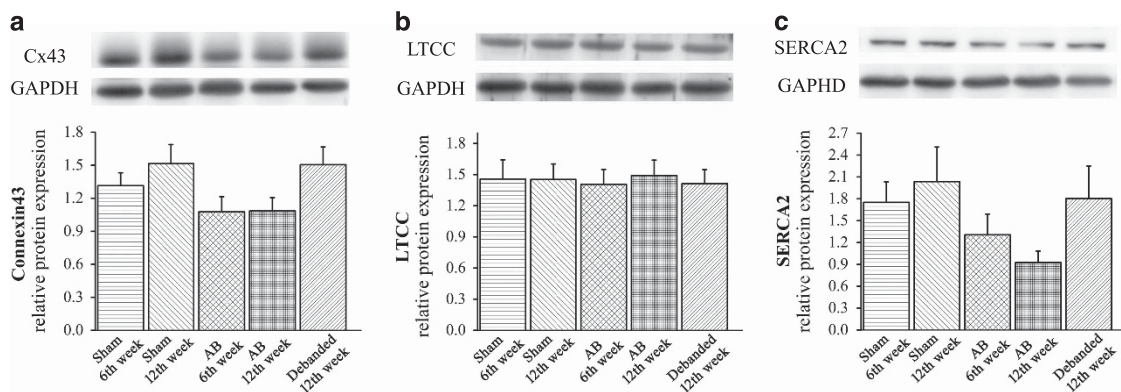


**Figure 5** Distinct protein expression alterations potentiate reverse electrical remodeling. Western blot analysis of Cx43 (a) showed a tendential reduction in the 6th and the 12th week aortic-banding group, without reaching a level of significance. The protein level of LTCC (b) remained unchanged in all experimental groups; however, the protein level of SERCA2 (c) was reduced with a strong tendency in the weeks 6 and 12 aortic-banded groups. Pressure unloading led to the restoration of these adverse alterations in protein expression levels (a–c). Cx43 indicates Connexin43, LTCC: L-type Ca<sup>2+</sup> Channel Protein  $\alpha$ 1C, SERCA2: sarcoplasmic/endoplasmic reticulum Ca<sup>2+</sup>-ATPase 2. All values are expressed as the means  $\pm$  s.e.m. \**P*<0.05 vs. sham, #*P*<0.05 vs. aortic-banded week 6, \$*P*<0.05 vs. aortic-banded week 12.



ion-channel distribution and function. In small mammals, the average resting heart rate is much higher while the APD is much shorter than in humans and ventricular repolarization relies on structurally and functionally different potassium channels.

Furthermore, the abdominal aortic-banded rat model has been widely acknowledged as a relevant rat model of pressure overload-induced pathological LVH. However, the artificial aortic constriction above the renal arteries might result in the hypoperfusion of the kidneys and therefore could subsequently potentiate the renin-angiotensin-aldosterone system,<sup>34</sup> which could result in volume retention. Therefore, it cannot be ruled out that in addition to the increased pressure overload, a subsequent volume overload may have contributed to the manifestation of pathological LVH in our investigation.

Although caution should be taken during the direct translation of our results into clinical practice, we believe that this study provides new insights into the mechanisms of reverse electrical remodeling and raises useful questions which in the future should be verified on human samples as well.

## CONFLICT OF INTEREST

The authors declare no conflict of interest.

## ACKNOWLEDGEMENTS

This study was supported by the Land Baden-Württemberg, Germany, by the Medical Faculty of the University of Heidelberg, Germany (to SK-I), by the National Research, Development and Innovation Office of Hungary (NKFI, NVKP-16-1-2016-0017), by the Hungarian Scientific Research Fund (OTKA 10555 to BM) and by the János Bolyai Research Scholarship of the Hungarian Academy of Sciences (to TR). The excellent technical assistance of Patricia Kraft, Tobias Mayer, Karin Sonnenberg, Lutz Hoffmann and Viktória Gregor is greatly acknowledged.

- McLenachan JM, Henderson E, Morris KI, Dargie HJ. Ventricular arrhythmias in patients with hypertensive left ventricular hypertrophy. *N Engl J Med* 1987; **317**: 787–792.
- Ahmed GU, Dong PH, Song G, Ball NA, Xu Y, Walsh RA, Chiamvimonvat N. Changes in Ca<sup>2+</sup> cycling proteins underlie cardiac action potential prolongation in a pressure-overloaded guinea pig model with cardiac hypertrophy and failure. *Circ Res* 2000; **86**: 558–570.
- Teunissen BE, Jongasma HJ, Bierhuizen MF. Regulation of myocardial connexins during hypertrophic remodelling. *Eur Heart J* 2004; **25**: 1979–1989.
- Wolk R. Arrhythmogenic mechanisms in left ventricular hypertrophy. *Europace* 2000; **2**: 216–223.
- Tomita F, Bassett AL, Myerburg RJ, Kimura S. Diminished transient outward currents in rat hypertrophied ventricular myocytes. *Circ Res* 1994; **75**: 296–303.
- Guo W, Li H, London B, Nerbonne JM. Functional consequences of elimination of i(to,f) and i(to,s): early afterdepolarizations, atrioventricular block, and ventricular arrhythmias in mice lacking Kv1.4 and expressing a dominant-negative Kv4 alpha subunit. *Circ Res* 2000; **87**: 73–79.
- Hill JA. Hypertrophic reprogramming of the left ventricle: translation to the ECG. *J Electrocardiol* 2012; **45**: 624–629.
- Kashani A, Barold SS. Significance of QRS complex duration in patients with heart failure. *J Am Coll Cardiol* 2005; **46**: 2183–2192.
- Tanaka-Esposito C, Varahan S, Jeyaraj D, Lu Y, Stambler BS. Eplerenone-mediated regression of electrical activation delays and myocardial fibrosis in heart failure. *J Cardiovasc Electrophysiol* 2014; **25**: 537–544.
- Wang Z, Kutschke W, Richardson KE, Karimi M, Hill JA. Electrical remodeling in pressure-overload cardiac hypertrophy: role of calcineurin. *Circulation* 2001; **104**: 1657–1663.
- Nikolaïdou T, Cai XJ, Stephenson RS, Yanni J, Lowe T, Atkinson AJ, Jones CB, Sardar R, Corno AF, Dobrzynski H, Withers PJ, Jarvis JC, Hart G, Boyett MR. Congestive heart failure leads to prolongation of the PR interval and atrioventricular junction enlargement and ion channel remodeling in the rabbit. *PLoS ONE* 2015; **10**: e0141452.
- Gao XM, Kiriazis H, Moore XL, Feng XH, Sheppard K, Dart A, Du XJ. Regression of pressure overload-induced left ventricular hypertrophy in mice. *Am J Physiol Heart Circ Physiol* 2005; **288**: H2702–H2707.
- Ruppert M, Korkmaz-Icoz S, Li S, Nemeth BT, Hegedus P, Brlecic P, Matyas C, Zorn M, Merkely B, Karck M, Radovits T, Szabo G. Myocardial reverse remodeling after pressure unloading is associated with maintained cardiac mechanoenergetics in a rat model of left ventricular hypertrophy. *Am J Physiol Heart Circ Physiol* 2016; **311**: H592–H603.
- Rials SJ, Wu Y, Ford N, Pauletto FJ, Abramson SV, Rubin AM, Marinchak RA, Kowey PR. Effect of left ventricular hypertrophy and its regression on ventricular electrophysiology and vulnerability to inducible arrhythmia in the feline heart. *Circulation* 1995; **91**: 426–430.
- Olah A, Nemeth BT, Matyas C, Hidi L, Lux A, Ruppert M, Kellermayer D, Sayour AA, Szabo L, Torok M, Meltzer A, Geller L, Merkely B, Radovits T. Physiological and pathological left ventricular hypertrophy of comparable degree is associated with characteristic differences of *in vivo* hemodynamics. *Am J Physiol Heart Circ Physiol* 2015; **310**: H587–H597.
- Nemeth BT, Matyas C, Olah A, Lux A, Hidi L, Ruppert M, Kellermayer D, Kokeny G, Szabo G, Merkely B, Radovits T. Cinaciguat prevents the development of pathologic hypertrophy in a rat model of left ventricular pressure overload. *Sci Rep* 2016; **6**: 37166.
- Kim HL, Kim YJ, Kim KH, Lee SP, Kim HK, Sohn DW, Oh BH, Park YB. Therapeutic effects of udenafil on pressure-overload cardiac hypertrophy. *Hypertens Res* 2015; **38**: 597–604.
- Korkmaz-Icoz S, Atmanli A, Radovits T, Li S, Hegedus P, Ruppert M, Brlecic P, Yoshikawa Y, Yasui H, Karck M, Szabo G. Administration of zinc complex of acetylsalicylic acid after the onset of myocardial injury protects the heart by upregulation of antioxidant enzymes. *J Physiol Sci* 2016; **66**: 113–125.
- Devereux RB, Alonso DR, Lutas EM, Gottlieb GJ, Campo E, Sachs I, Reichek N. Echocardiographic assessment of left ventricular hypertrophy: comparison to necropsy findings. *Am J Cardiol* 1986; **57**: 450–458.
- Pombo JF, Troy BL, Russell RO Jr. Left ventricular volumes and ejection fraction by echocardiography. *Circulation* 1971; **43**: 480–490.
- Kmecova J, Klimas J. Heart rate correction of the QT duration in rats. *Eur J Pharmacol* 2010; **641**: 187–192.
- Korkmaz-Icoz S, Vater A, Li S, Lehner A, Radovits T, Hegedus P, Ruppert M, Brlecic P, Zorn M, Karck M, Szabo G. Mild type 2 diabetes mellitus improves remote endothelial dysfunction after acute myocardial infarction. *J Diabetes Complications* 2015; **29**: 1253–1260.
- Boulakissil M, Noorman M, Engelen MA, van Veen TA, Vos MA, de Bakker JM, van Rijen HV. Longitudinal arrhythmogenic remodelling in a mouse model of long-standing pressure overload. *Neth Heart J* 2010; **18**: 509–515.
- Klimas J, Kruzliak P, Rabkin SW. Modulation of the QT interval duration in hypertension with antihypertensive treatment. *Hypertens Res* 2015; **38**: 447–454.
- Farrar AK, Hazari MS, Cascio WE. The utility of the small rodent electrocardiogram in toxicology. *Toxicol Sci* 2011; **121**: 11–30.
- Schroder F, Handrock R, Beuckelmann DJ, Hirt S, Hullin R, Priebe L, Schwinger RH, Weil J, Herzog S. Increased availability and open probability of single L-type calcium channels from failing compared with nonfailing human ventricle. *Circulation* 1998; **98**: 969–976.
- Chen X, Piacentino V 3rd, Furukawa S, Goldman B, Margulies KB, Houser SR. L-type Ca<sup>2+</sup> channel density and regulation are altered in failing human ventricular myocytes and recover after support with mechanical assist devices. *Circ Res* 2002; **91**: 517–524.
- Nagasawa K, Takahashi K, Matsuura N, Takatsu M, Hattori T, Watanabe S, Harada E, Niinuma K, Murohara T, Nagata K. Comparative effects of valsartan in combination with cilnidipine or amlodipine on cardiac remodeling and diastolic dysfunction in Dahl salt-sensitive rats. *Hypertens Res* 2015; **38**: 39–47.
- Juliano S, Fisher SG, Karasik PE, Fletcher RD, Singh SN. Department of Veterans Affairs Survival Trial of Antiarrhythmic Therapy in Congestive Heart F. QRS duration and mortality in patients with congestive heart failure. *Am Heart J* 2002; **143**: 1085–1091.
- Sohl G, Willecke K. Gap junctions and the connexin protein family. *Cardiovasc Res* 2004; **62**: 228–232.
- Kostin S, Dammer S, Hein S, Klovekorn WP, Bauer EP, Schaper J. Connexin 43 expression and distribution in compensated and decompensated cardiac hypertrophy in patients with aortic stenosis. *Cardiovasc Res* 2004; **62**: 426–436.
- Kostin S, Rieger M, Dammer S, Hein S, Richter M, Klovekorn WP, Bauer EP, Schaper J. Gap junction remodeling and altered connexin43 expression in the failing human heart. *Mol Cell Biochem* 2003; **242**: 135–144.
- Emdad L, Uzzaman M, Takagishi Y, Honjo H, Uchida T, Severs NJ, Kodama I, Murata Y. Gap junction remodeling in hypertrophied left ventricles of aortic-banded rats: prevention by angiotensin II type 1 receptor blockade. *J Mol Cell Cardiol* 2001; **33**: 219–231.
- Massart PE, Donckier J, Kyselovic J, Godfraind T, Heyndrickx GR, Wibo M. Carvedilol and lacidipine prevent cardiac hypertrophy and endothelin-1 gene overexpression after aortic banding. *Hypertension* 1999; **34**: 1197–1201.